WDS'05 Proceedings of Contributed Papers, Part III, 518–523, 2005. ISBN 80-86732-59-2 © MATFYZPRESS

Superparamagnetism of Co-Ferrite Nanoparticles

J.P. Vejpravová and V. Sechovský

Charles University, Faculty of Mathematics and Physics, Prague, Czech Republic.

D. Nižňanský

Charles University, Faculty of Natural Sciences, Prague, Czech Republic.

J. Plocek and A. Hutlová

Academy of Sciences of the Czech Republic, Prague, Czech Republic.

J.-L. Rehspringer

Institut de Physique et Chimie des Matériaux de Strasbourg, Strasbourg, France

Abstract. Well-defined $CoFe_2O_4$ nanoparticles embedded in amorphous SiO_2 matrix have been synthesized by sol-gel method, characterized and investigated by Mössbauer spectroscopy and magnetic measurements. The mean particle size was found to increase from 3 to 15 nm by varying the temperature of a subsequent annealing from 800 to 1100 °C. The composites exhibited superparamagnetic behavior with the blocking temperature increasing with the mean particle size. The frequency dependent AC susceptibility was found to obey the Néel - Arrhenius law. Both observations are compatible with a model of non-interacting randomly oriented single-domain particles.

1. Introduction

Superparamagnetism is a phenomenon by which magnetic materials may exhibit a behavior similar to paramagnetism at temperatures below the Curie or the Néel temperature. Superparamagnets consist of individual (single) magnetic domains of elements (or compounds) that have ferromagnetic properties in bulk.

Theoretical predictions concerning energetic stability of a single magnetic domain were established by Kittel in 1946 [1], defining a certain critical size of a particle (typically nanometers for usual ferromagnets); in smaller particles formation of a single ferromagnetic domain is preferred. Moreover, it was shown by Néel, that at temperatures above the so-called blocking temperature T_{B}, a stable bulk magnetization cannot be established due to thermal fluctuations acting on small particles and consequently the system exhibits superparamagnetism (SPM) [2]. At low temperatures (below $\mathrm{T_B}$) the thermal fluctuations do not dominate and magnetic moments of SPM particles 'freeze' in random orientation and cannot rotate freely.

Already the first model of magnetization reversal in a single-domain particle (assuming coherent rotation of the magnetic domain moment) presented by Stoner and Wohlfarth [3] suggested existence of high coercivity fields below T_B - when the energy of magnetocrystalline anisotropy becomes comparable with the thermal activation energy, the direction of the particle magnetic moment starts to fluctuate and goes through a rapid superparamagnetic relaxation. At temperatures above T_B (supposing a system of uniform non-interacting nanoparticles) the thermal effects allow flips of magnetic moments between the easy magnetization directions by getting over the energy barriers in zero field and consequently the $H_C = 0$. At temperatures ($\mathrm{T} < T_{\mathrm{B}}$) the thermal activation cannot overcome the magnetocrystalline anisotropy and the magnetic moment of each particle rotates from the field direction back to the nearest easy magnetization axis that yields a non-zero coercivity field. Since the nanoparticles and so the corresponding easy magnetization directions are randomly oriented, the total magnetization is naturally reduced with increasing temperature.

Due to enormous application potential of nanoparticles the demand of their manufacturing rises despite of persisting difficulties in larger-scale production. The high coercivity fields revealed for magnetic nanoparticle system [4] makes these materials interesting for applications in the field of high-density magnetic media. Recently, the superparamagnetic behavior has been also employed in biomedicine by means of hyperthermia (malign cell heat treatment) [5]. So far, many studies of elemental nanoparticles

(Ni, Co, Fe) have been published e.g. [6; 7], while overall reports on ferrite-based systems are still few in number. One reason is that to obtain isolated ferrite nanoparticles is often a crucial problem namely due to difficult control of the particle shape and size distribution [8]. Promising candidates are cobalt ferrite composites because of high coercivity fields H_c and saturated magnetization M_s values provided [9; 10]. In this work, we present details of fabrication, characterization and selected magnetic characteristics of well-defined $CoFe_2O_4$ nanoparticles embed in amorphous SiO_2 matrix.

2. Experimental

2.1. Synthesis and Characterization

We used a conventional sol-gel method [11] with TEOS (Tetraethyl-orthosilicate), HNO_3 as an acid catalyst, formamide as a modifier, and methanol as a solvent for silica matrix preparation. $Fe(NO_3)_3.9H_2O$ and $Co(NO_3)_2.6H_2O$ were first dissolved in methanol and the Si/Fe molar ratio was fixed to 100/15 (gelation time - 24 hours at 40 °C. The samples were left two days for ageing followed by progressive drying at 40 °C for three days in flowing N_2-atmosphere. After drying, the samples were preheated at 300 °C in vacuum for two hours and then under atmospheric pressure at one of the following temperatures: 800, 900, 1000 and 1100 °C and finally labelled according to the last annealing temperature as S800 - S1100, respectively.

A high-resolution transmission electron microscope Topcon was used for the direct observation of the particle appearance (Fig. 1a). Particle size determination was determined using the Scion Images software. The nanocomposites show well-defined grains with the increasing mean particle size from 3 nm up to 15 nm in diameter according to the annealing temperature for the S800 - S1100 samples, respectively, see Table 1.

All samples were characterized by powder X-ray diffraction using a Siemens D500 diffractometer equipped with a cobalt anode ($\lambda(CoK\alpha) = 1.7890$ Å) and a quartz primary monochromator in order to identify the phase composition. The XRD patterns of the samples after final thermal treatment are shown in Fig. 1b. A tendency of crystallization as a function of heating temperature is reflected by a broad diffraction peak at around 20 ° (2 θ). The process of crystallization as a function of heating temperature can be followed from the FWHM (full width at half maximum) of diffraction peaks, which follows the Scherrer equation, and it also permitted us to estimate the particle size, see Table 1. [12].

a b

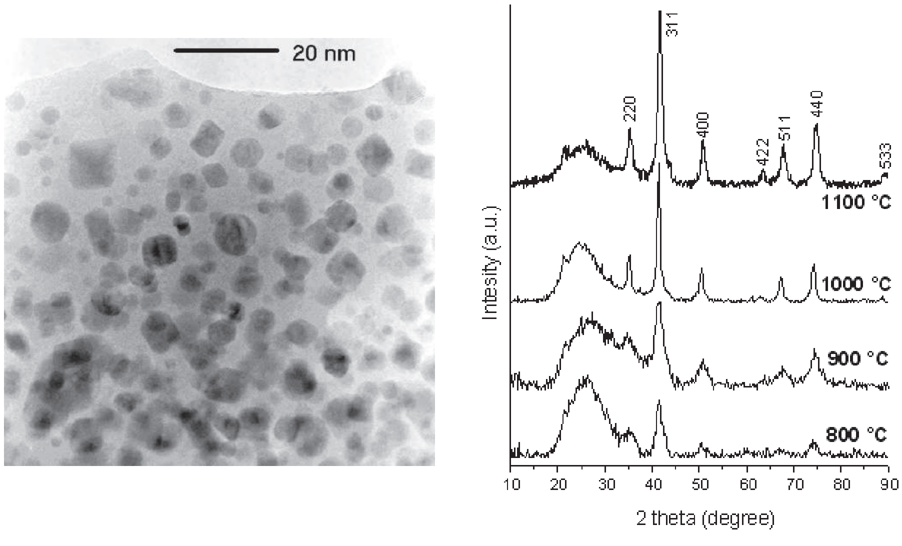

Figure 1. a - HR TEM image of S1000 sample. b - XRD patterns of S800 - S1100 samples. The extended maximum at $\sim 25°$ corresponds to the amorphous silica matrix contribution.

2.2. Mössbauer spectra

The Mössbauer spectra measurement was done in the transmission mode with ^{57}Co diffused into a Rh matrix as the source moving with constant acceleration. The spectrometer was calibrated by means of a standard α-Fe foil and the isomer shift was expressed with respect to this standard at 293 K. The spectra were recorded at several different temperatures in magnetic fields up to 5 T applied perpendicular to the direction of the γ-ray emission and fitted with the help of the NORMOS program.

2.3. Magnetic measurements

The DC magnetization (M) as a function of temperature (2 - 350 K) and magnetic field (0 - 14 T) together with the AC susceptibility (frequency range 83 - 8333 Hz, DC amplitude 1 mT) were measured in the PPMS 14T and PPMS 9T devices (Quantum Design, San Diego). The temperature dependencies of the DC magnetization were measured at 50mT; first after cooling the sample in zero magnetic field (ZFC curve) followed by cooling the sample under applied magnetic field (FC curve) and measuring during heating at the same field.

3. Results and Discussion

3.1. Mössbauer spectra

The Mössbauer spectrum of S900 sample suggests superparamagnetism at room temperature (no sextet is observed), while after cooling to 140 K partial magnetic arrangement is observed (sextet appearance). Simultaneous occurrence of both the sextet and the doublet reflects a certain size distribution of the $CoFe_2O_4$ particles resulting in distribution of the blocking temperatures. At 4.2 K a complete ferromagnetic ordering of the magnetic moments in Co ferrite particles is detected. Due to a very strong overlap of the subspectra one cannot distinguish between the iron positions in the spinel structure (Td - tetrahedral, Oh - octahedral sites). When we take generally accepted recoilless factors for the spinel structure (f_{Td} : f_{Oh} = 1.2) [13] into account we can express real formula of our spinel as follow: $(Co_{0.41}Fe_{0.59})$ $[Co_{0.59}Fe_{1.41}]O_4$. The great deviation from ideal structure can be explained by the presence of very small particle- fraction and non-negligible influence of surface atoms. The spectra of the S1000 sample yield occurrence of both sextet and doublet, which can be again explained by a certain size distribution of the $CoFe_2O_4$ particles reflecting partly ferromagnetic sample at 293 K. At 4.2 K in 5 T the spectrum shows magnetically ordered structure of cobalt ferrite (no doublet is present). Moreover, there is again a deviation from the ideal inverse spinel structure (area ratio (S_{Td} : S_{Oh}) differs from 1.2).

3.2. Magnetization study - coercivity and superparamagnetism

The furcation of ZFC and FC curves at a certain temperature (denoted as T_{diff} in our case) is one of the characteristic features of a superparamagnetic (SPM) system as seen in Fig. 2 for S800. However, the coinciding broad maximum observed on the ZFC curve occurs at a slightly lower temperature (symbolized as $T_{\max}$) than T_{diff}. Such behavior usually signalizes a certain particle size distribution in the nanocomposite; while a fraction of the largest particles already freeze at T_{diff}, the majority fraction of the nanoparticles in the sample is being blocked at $T_{\max}$ resulting in a distribution of the blocking temperatures T_B in the sample; the distinctive values (at T_{diff} and $T_{\max}$, respectively) of the blocking temperatures T_B for all four samples are summarized in Table 1. The value of $T_{\max}$ and T_{diff} monotonously increases with the increasing mean size of the particles (correspondingly to the higher annealing temperatures) as expected.

At low temperatures, the value of coercivity field H_c (symmetric for opposite polarity of magnetic field: H_c = -H_c) is increasing with increasing size of particles (despite of slightly varying value of saturated magnetization from $M_s \sim 19$ Am^{2}kg^{-1} for S1100 to $M_s \sim 16$ Am^{2}kg^{-1} for S800 at 2K), see Fig. 3. At low temperatures coercivity of a system of non-interacting and randomly oriented particles is expected to follow the relation:

$$H_{\mathrm{C}}(T) = H_{\mathrm{C0}}\left[1 - \left(\frac{T}{T_{\mathrm{B}}}\right)^{1/2}\right] \tag{1}$$

An extrapolated value of H_{C0}, together with T_{B} (summarized in Table 1.) have been derived for all samples. An estimation of nanoparticle mean radius was obtained using general formulas:

$$T_B = \frac{K < V >}{25 k_B} \tag{2}$$

where K is the first-order magneto-crystalline anisotropy constant of bulk $CoFe_2O_4$ ferrite [14], supposing to be temperature independent, $< V >$ is the average particle volume ($\mu = M_s^{bulk} < V >$), M_s^{bulk} is the saturated magnetization of bulk $CoFe_2O_4$, T_B and k_B have usual meaning . The values of radii of the nanoparticles are in a good agreement with those obtained by other methods.

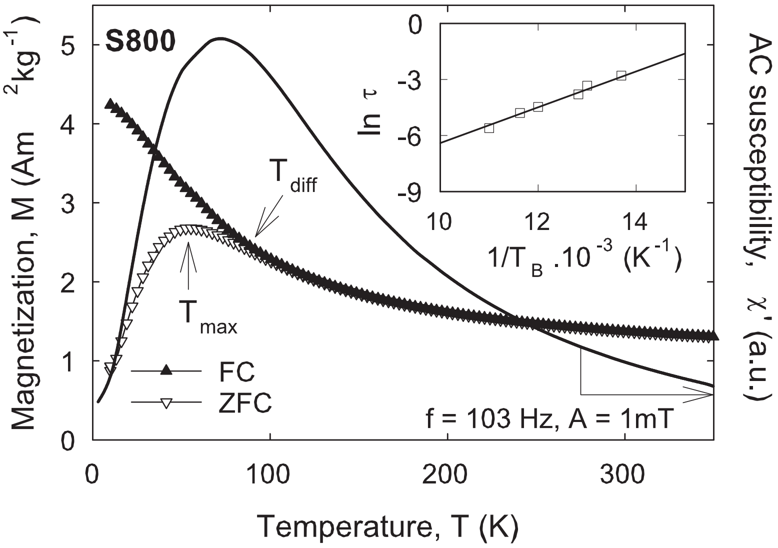

Figure 2. Temperature dependence of ZFC - FC magnetization of S800 sample at 50 mT in comparison with that of AC susceptibility (real part, χ'). The inset shows the logarithmic dependence of the relaxation time τ against the inverse blocking temperature T_B according to the Néel - Arrhenius law.

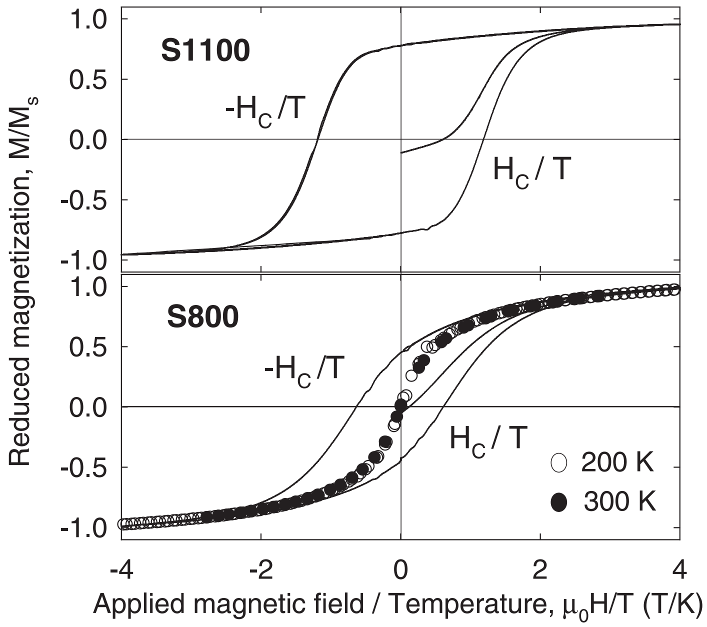

Figure 3. Virgin magnetization curves and hysteresis loops of S800 and S1100 samples measured at 2 K (solid line) together with unhysteretic curves of S800 in SPM state. The deviation of the virgin curves from the expected zero value at 0 T is due to a small fraction of the sample being already magnetized.

The SPM behavior of these samples above T_B has been confirmed when plotting M/M_s vs. $\mu_0 H/T$ (M_s is the saturated magnetization) resulting in a universal curve seen in inset, Fig. 3. This scaling is consistent with the SPM response, although it is correct only in low fields [6; 15]. The contribution from the SPM nanoparticles to the total magnetization can be described by:

$$M = M_s L(x), x = \left(\frac{\mu H}{k_B T}\right), \tag{3}$$

where M_s is the saturation magnetization of N particles with magnetic moment μ and $L(x)$ is the Langevin function. This expression is valid only for a system of monodisperse noninteracting particles. However, since real systems have a non-negligible distribution of magnetic moments, the magnetization of SPM grains is better described as a weighted sum of Langevin functions [6; 15]:

$$M = \int_0^\infty L(x) M_S dx, x = \left(\frac{\mu H}{k_\mathrm{B} T}\right), \tag{4}$$

where M_S is given by:

$$M_S = \int_0^\infty \frac{1}{\sqrt{2\pi}\mu\sigma} \exp\left(-\frac{\ln^2(\mu/\mu_0)}{2\sigma^2}\right) d\mu, \tag{5}$$

where σ is the log-normal distribution width and μ_0 is the median of the distribution related to the average magnetic moment μ_m by:

$$\mu_m = \mu_0 \exp(-\frac{\sigma}{2}). \tag{6}$$

The resulting parameters obtained by the fit to experimental data of S800, S900 and S1000 are summarized in Table 1. The fit of a single Langevin function provided generally higher values of μ_m accompanied by a much worse standard deviation and therefore it is not presented.

3.3. Dynamic properties AC susceptibility

The temperature dependence of the AC susceptibility(χ', χ") shows characteristic maxima corresponding to the blocking temperatures T_B(derived from the maximum position at 103 Hz are summarized in Table 1.), which are shifted to higher temperatures with increasing frequency as depicted in Fig. 2 for S800. This observation corroborates the idea that the nanoparticles behave like non-interacting and single-domain species excluding any additional significant dipole-dipole or inter-particle interactions.

A useful criterion for classifying the observed freezing process is the empirical parameter Φ [16], which represents the relative shift of the blocking temperature per a frequency decade:

$$\Phi = \frac{\Delta T_f}{T_f \Delta \log_{10}(f)}, \tag{7}$$

where ΔT_f is the difference between the blocking temperature measured in the $\Delta \log_{10}(f)$, f is the AC magnetic field frequency. For the both the S800 and S900 samples we have obtained the value of $\Phi = 0.09$, which is very closed to the 0.1 value found for the SPM system. On the other hand, smaller values of Φ are usually caused by the spin-glass-like behavior of the nanoparticle surface or simply due to non-negligible interparticle interactions [17; 18].

The linear dependence of lnf vs $1/T_\mathrm{B}$ follows the Néel-Arrhenius law for the S800 and S900 samples, see the inset in Fig. 2:

$$\tau = \tau_0 \exp\frac{E_\mathrm{a}}{k_\mathrm{B} T}, \tag{8}$$

where τ is the relaxation time at frequency f, E_a is the anisotropy energy barrier and τ_0 is the characyeristic relaxation time and ranges typically from 10^{-9} to 10^{-11} s for SPM systems [19]. In the absence of the external magnetic field, the energy barrier E_a is proportional to the particle volume V and can be expressed as $E_a = K_\mathrm{eff} V \sin^2\theta$, where K_eff is an effective magnetic anisotropy constant and θ is the angle between the easy magnetization axis of the particle and its magnetic moment direction. The resulting values of τ_0, E_a and K_eff are 1.8×10^{-8} s and 1.3×10^{-8}s; 1227 K and 920 K, 4×10^{-1} J/m^3 and 3×10^{-1} J/m^3 for the S800 and S900 samples, respectively. The resulting effective anisotropy is practically the same as the first-order anisotropy bulk constant (3.5×10^{-1} J/m^3 [14]) indicating negligible surface effects and dipolar interaction between nanoparticles [18].

4. Conclusions

In summary we have prepared series of $CoFe_2O_4$ nanocomposites embed in amorphous SiO_2 matrix. Irregular occupation of Fe positions in the inverse-spinel structure has been observed by the Mössbauer spectroscopy under magnetic field. Magnetic behavior of the composites follows the Neél theory of single domain noninteracting entities exhibiting SPM behavior above T_B increasing with the temperature of the heat treatment according to the mean particle size. Below T_B, appreciably high values of coercivity develops increasing up to $H_{C0} = 2.9$ T for S1100.

Acknowledgments. This work was supported by the research plan MSM0021620834 financed by the Ministry of Education of the Czech Republic. The work was also supported by the Grant Agency of the ASCR under the Project No.:KJB4032402.

Table 1. Summary of magnetic characteristics: blocking temperatures T_B (determined from AC susceptibility, T_{diff}, T_{max}, eq. (1), average magnetic moment per particle μ_m, average particle diameter (R) obtained by the fit of the weighted sum of Langevin functions (L), mean particle diameter observed by TEM and from FWHM, extrapolated coercivity field H_{C0}.

Sample	T_B(K) AC	T_B(K) T_{diff}	T_B(K) T_{max}	T_B(K) eq. (1)	$\mu_m(\mu_B)$ L	R (nm) L	R (nm) TEM/FWHM	H_{C0} eq. (1)
S800	87	92	50	80	4700	1.5	1.5/2.0	1.9
S900	107	116	60	105	5700	2	2.0/3.0	1.8
S1000	290	305	180	275	8100	5.5	5.5/4.0	2.2
S1100	x	350	300	295	x	7.5	x/8.0	2.9

References

[1] C. Kittel, Phys. Rev. **70**, 965 (1946).
[2] L. Néel, Ann. Grophys. (C.N.S.R.) **5**, 99 (1949).
[3] E.C. Stoner, E.P. Wohlfarth. Philos. Trans. R. Soc. London, Ser. A, **240**, 599 (1948).
[4] L. Lu, M.L. Sui, K. Lu, Science **287**, 1463 (2000).
[5] A. Jordan, R. Scholz, P. Wust, H. Fahling, R. Felix, J. Magn. Magn. Mater. **201**, 413 (1999).
[6] F.C. Fonseca, G.F. Gya,R.F. Jardim, R. Muccillo, N.L.V. Carreno, E. Longo, E.R. Leite, Phys. Rev. B **66**, 104406 (2002).
[7] A. Fnidiki, C. Dorien, F. Richomme, J. Teillet, D. Lemarchand, N.H. Duc, J. Ben Youssef, H. Le. Gall, Journal of Magn. Magn. Mater. **262**, 368 (2003).
[8] L.D. Tung, V. Kolesnichenko, D. Caruntu, N.H. Chou, C.J. O'Connor, L. Spinu, Journal of Appl. Phys. **93**, 7486 (2003).
[9] A. Hutlová, D. Nižňanský, J.-L. Rehspringer, C. Estournes, M. Kurmoo, Advanced Matt. **19**, c5305 (2003).
[10] L.A. Garcia-Cerda, V.A. Torres-Garcia, J.A. Matutes-Aquino, O.E. Ayala-Valenzuela, Journal of Alloys and Compounds **369**, 148 (2004).
[11] R.F.S. Lenza, W.L.Vasconcelos, Materials Research, **4**, 189 (2001).
[12] R. Jenkins and R. L. Snyder, *Introduction to X-ray powder diffractometry*, John Willey & Sons, Inc., New York, (1996).
[13] J.L. Dormann, D. Fiorani and S. Vitticoli, *Proc. Int. Conf. Applications of Mossbauer Effects (Jaipur) (New Delhi: INSA)*, p. 206 (1981).
[14] S. Krupička, *Fyzika feritu a příbuzných kysličníku*, Academia, Prague 1980.
[15] E.F. Ferrari, F.C.S. da Silva, M. Knobel, Phys. Rev. B **56**, 6068 (1997).
[16] G.F. Goya, T.S. Berquo, F.C. Fonseca, M.P. Morales, Journal of Appl. Phys. **94**, 3520 (2003).
[17] J.L. Dormann, D. Fiorani, E. tronc, Adv. Chem. Phys. **XCVIII**, 326 (1997).
[18] G.F. Goya, IEEE Trans. Magn.**38**, 2610 (2002).
[19] G. Xiao, S.H. Liou, A. Levy, J.N. Taylor, C.L. Chien, Phys. Rev. B **34**, 7573 (1986).